THE JOURNAL OF PHYSICAL CHEMISTRY C

pubs.acs.org/JPCC Article

Reaction Kinetics and Influence of Film Morphology on the Oxidation of Propene Thin Films by O(^{3}P) Atomic Oxygen

Michelle R. Brann, Rebecca S. Thompson, and S. J. Sibener*

Cite This: https://dx.doi.org/10.1021/acs.jpcc.9b11439 Read Online

ACCESS | Metrics & More | Article Recommendations

ABSTRACT: We present results detailing the oxidative reactivity of condensed propene thin films, with particular attention to epoxide product formation because of its importance in the industrial production of polyurethane plastics and the trace presence of these species in the interstellar medium. These studies were conducted in a state-of-the-art ultrahigh vacuum scattering instrument equipped for operation with cryogenic substrate temperatures. After exposing films to a supersonic beam of ground-state atomic oxygen, O(^{3}P), generated from a radio frequency plasma source, reflection absorption infrared (RAIR) spectra confirm significant propene reactivity, yielding products including propylene oxide, propanal, and a small amount of acetone. In addition to identifying these primary products, we discuss experimentally determined activation energy barriers for reaction in the condensed propene system. Interestingly, we identify significant differences in propene film crystallinity as a result of substrate deposition temperature; lower deposition temperatures (<44 K) yield a more amorphous film, whereas higher temperatures (>59 K) yield a more ordered, crystalline film. Very little oxidative reactivity is observed in the amorphous propene film, suggesting that the film structure has a substantial impact on observed reactivity by impeding or allowing efficient O(^{3}P) diffusion. Overall, this work provides fundamental mechanistic insights into the diffusion and reactivity of atomic oxygen in condensed films of small, unsaturated hydrocarbons. The results also emphasize limitations of condensed-phase reactions that rely on reactant diffusion; film composition, morphology, and thickness can significantly limit reactivity despite low reaction barriers.

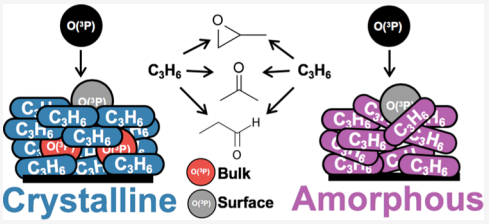

INTRODUCTION

The reaction of atomic oxygen, O(^{3}P), with small alkenes is important across many fields including smog formation in the atmosphere, combustion processes, and chemical complexity in astrophysical ices.[1,2] These reactions also play a critical role in the formation of polycyclic aromatic hydrocarbons and soot.[3] Additionally, the products formed from oxygen addition across double bonds are often significant industrial intermediates. Propylene oxide, for example, is a key intermediate in the manufacturing of polyurethane plastics and other products.[4,5] It is one of the top chemicals produced worldwide by mass,[6] and there is immense interest in optimizing the economic and environmental efficiency of its production.[7−9]

The gas-phase reaction between alkenes (including propene) and oxygen has been well-studied, beginning as early as the 1950s.[10−14] It is well established that the reaction begins with oxygen addition across the double bond, forming a triplet biradical intermediate. This primary product species then progresses through a number of reaction channels including intersystem crossing (ISC) from the triplet to the singlet potential energy surface (PES) to form singlet products. Recently, a comprehensive study from Leonori et al. used crossed molecular beams and complementary ab initio electronic structure calculations to identify complete branching ratios, energetic barriers, and PESs for the O(^{3}P) + propene reaction.[15,16] This study and others have highlighted the temperature-dependent role of ISC in the gas-phase reaction; the fraction of products formed via ISC decreases with increasing temperature.[12,15,16] Despite this rigorous work in the gas phase, there still remains limited mechanistic and kinetic data available for the oxidation of condensed alkene films. In the few early studies of this system,[17−20] primary products and reaction rates were identified, but the experimental conditions utilized thick, uncharacterized propene films and were limited to temperatures above 70 K (propene phase may have been unclear).

Understanding reactions between condensed alkenes and oxygen at cold temperatures is also important for astrophysical applications because of the trace presence of the species in the interstellar medium.[21] It is thought that reactions on interstellar dust grains below 77 K facilitate the formation of many such molecules with abundances that cannot be explained by gas-phase chemistry alone.[22−24] To date, only gaseous propene has been observed in a dark interstellar

Received: December 10, 2019
Revised: February 16, 2020

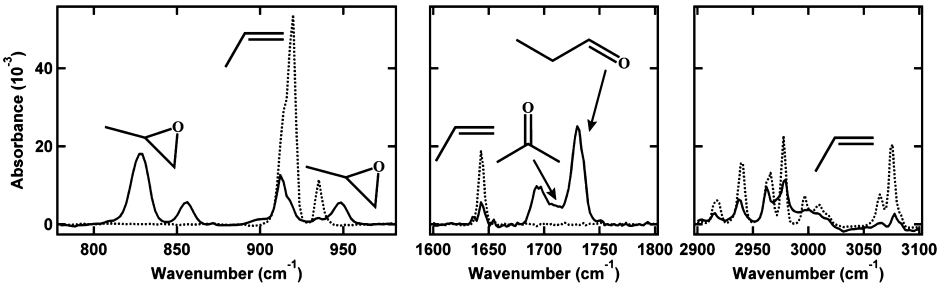

Figure 1. RAIR spectra of characteristic regions of a 66-layer propene film before (dashed line) and after exposure to $O(^3P)$ (solid line, total exposure $\approx 1 \times 10^{18}$ atoms cm^{-2}). As a result of exposure, the total signal intensity is observed to decrease for the CH_2 wagging (919 and 914 cm^{-1}, a), C=C stretching (1643 cm^{-1}, b), and CH, CH_2 and CH_3 stretching (3009, 3075, 2977, 2939, and 2964 cm^{-1}, c) modes of propene. Growth of new peaks upon exposure to $O(^3P)$ corresponding to propylene oxide (830 cm^{-1}, a), acetone (1709 cm^{-1}, b), and propanal (1730 cm^{-1} and 1693 cm^{-1}, b).

cloud[25] and on Titan,[26] but molecules formed on dust grains (possibly due to exposure to ionizing radiation)[27] could desorb and contribute to these measured gas-phase concentrations.[28] Additionally, propylene oxide, one of the major products in the $O(^3P)$ + propene reaction, has been detected spectroscopically in the interstellar medium[29] as well as produced in a laboratory simulation experiment by exposure of propylene ices at 5 K to energetic electrons.[30] Such studies indicate that oxygen atom addition and insertion reaction pathways could activate a novel channel for chemical complexity in ices that are too cold for radicals to diffuse and react.[31,32]

In this work, a radio frequency (RF) plasma source is used to generate a supersonic expansion of ground-state atomic oxygen, $O(^3P)$, which is then exposed to condensed propene films under ultrahigh vacuum (UHV) conditions. We track reaction product formation in real time with in situ reflection absorption infrared spectroscopy (RAIRS), which allows us to determine the activation energy for this process. We find that in the condensed phase, propene reacts readily with $O(^3P)$ to form primarily the singlet partial oxidation products propylene oxide and propanal. Additionally, we present the first study highlighting the specific impact of alkene film morphology on oxidative reactivity. Specifically, oxygen is unable to react with more disordered, amorphous propene films.

Overall, this work provides fundamental insights into the diffusion and reactivity of ground-state atomic oxygen in condensed films of small, unsaturated hydrocarbons. By employing cryogenic conditions and thin films of propene, we can simulate interstellar conditions which can aid in modeling reactivity on interstellar dust grains. Additionally, the kinetic and mechanistic details gained from this reaction will inform polyurethane plastic manufacturing. This work also broadly highlights the possible challenges with condensed-phase reactivity in which film structure and morphology may significantly limit reactant diffusion and reactivity in thicker films.

EXPERIMENTAL SECTION

All experiments were conducted in a molecular beam scattering instrument that has been previously discussed in detail.[33] Briefly, this instrument consists of a UHV chamber with a base pressure of 10^{-10} Torr connected to a triply differentially pumped molecular beamline. Inside the chamber, a state-of-the-art, helium-cooled, and vibrationally isolated sample manipulator (Advanced Research Systems) enables precise and accurate temperature control of the Au(111) sample substrate between 20 and 800 K. The crystal is exposed to the beam and monitored in real time with in situ RAIRS.

All RAIR spectra were analyzed with Gaussian peaks atop cubic baselines. Spectra were acquired with a Nicolet 6700 infrared spectrophotometer (Thermo Fisher) using p-polarized IR radiation incident at 75° from the surface of a Au(111) sample substrate and collected in a liquid nitrogen-cooled mercury cadmium telluride (MCT/A) detector. Each RAIR spectrum is an average of 300−500 scans taken using a 4 cm^{-1} resolution with a clean Au(111) sample used as a reference background. Between experiments, the Au(111) crystal was sputtered and thermally annealed in vacuum using 1 kV Ar^+ ions ($1-2 \times 10^{-5}$ Torr Ar backfilled into the chamber) directed at the crystal by an ion gun, while the surface temperature was held at 770 K for 15 min.

Propene was dosed on the Au(111) substrate via beam deposition at surface temperatures ranging from 44 to 59 K, where propene desorption is negligible. Dosing conditions resulted in a typical incident propene flux of 2.6×10^{15} molecules cm^{-2} s^{-1}, corresponding to a deposition rate of approximated 2.4 layers s^{-1} [assuming one monolayer (ML) is roughly 10^{15} molecules cm^{-2}].[34] Propene flux was initially determined by measuring the pressure rise with a nude Bayard−Alpert ion gauge calibrated to N_2 for a neat propene beam open to the chamber. The flux was then calculated by taking into account the relative gauge sensitivity to propene[35] and N_2[36] along with the chamber pumping speed and the spot size of the beam on the Au(111) crystal. We performed this measurement and calculation at room temperature to ensure that no additional pumping capacity was added by the cold sample manipulator. Following this measurement, we used the same beam to establish a conversion to propene film thickness by monitoring propene growth on the cold crystal via RAIRS as a function of exposure and calculating an absorption cross section for the $=CH_2$ wagging mode (γ_w), composed of two peaks: a large, sharp peak at 919 cm^{-1} and a smaller shoulder at 914 cm^{-1}. Our calculated cross section is in good agreement with previously reported values.[37−40] Propene film thicknesses are herein reported in layers; films throughout this study ranged from 10 to 240 layers (specific thicknesses are specified in the text). The beam source was thoroughly pumped out and purged prior to turning on the oxygen source to avoid trace propene contaminants during exposure.

An RF plasma source described in detail previously[41] was used to generate atomic oxygen in its ground state, $O(^3P)$. Igniting and expanding a 5% O_2 in Ne mixture through a water-cooled quartz nozzle led to 25−40% O_2 dissociation to

https://dx.doi.org/10.1021/acs.jpcc.9b11439
J. Phys. Chem. C XXXX, XXX, XXX−XXX

$O(^3P)$. We note that by selecting a low backing pressure (60 Torr) and a low RF power (100 W) and employing a 2000 V/cm deflecting plate region in the second differential beam chamber, our beam is essentially devoid of O^+ and $O(^1D)$[42,43] and is primarily composed of $O(^3P)$, nondissociated O_2, and Ne. The beam is characterized using time-of-flight (TOF) techniques to determine the flux and average kinetic energy. O_2 flux was determined in a manner similar to that of propene (see above) using a neat O_2 beam and the relative ionization sensitivity to O_2 and N_2.[36,44] O_2 flux is further scaled to reflect dissociation into $O(^3P)$ using the relative intensities of m/z = 16 to m/z = 32 established from square wave modulated TOF spectra of the incident beam.[41] Typical experimental conditions result in an $O(^3P)$ flux of 8.4×10^{14} atoms cm^{-2} s^1 and a translational energy of 0.12 eV. The beam energy widths are approximately 0.06 eV. While it would be desirable to explore the reaction with higher incident translational energies by substituting a seeded mixture of O_2 in He, doing so would reduce O_2 dissociation and introduce $O(^1D)$ to the beam, which is a more reactive species.[45] Thus, for this experiment, 5% O_2 in Ne remains the optimal gas mixture.

RESULTS AND DISCUSSION

Spectral Evidence of Reactivity and Product Formation. Condensed propene is observed to react readily with $O(^3P)$. Figure 1 shows typical RAIR spectra of a 66-layer propene film adsorbed on Au(111) at 54 K before and after extended exposure to $O(^3P)$. Prior to exposure, spectral features are easily correlated with gas-phase and condensed-phase propene peak assignments.[39,40,46−50] As shown by the dashed line in Figure 1a, the most intense features at 919 and 914 cm^{-1} are assigned to the $=CH_2$ wagging mode of propene (γ_w) with a smaller feature at 1003 cm^{-1} corresponding to the CC bend.[49−51] Unless otherwise stated, changes in the integrated areas of the features at 914 and 919 cm^{-1} are used throughout the rest of this study to track the propene reaction progress (generally corresponding to the reaction of the propene double bond). A second region is highlighted in Figure 1b at 1643 cm^{-1}, corresponding to the propene C=C stretch.[52] A third region highlighted in Figure 1c shows additional CH, CH_2, and CH_3 stretching modes that are smaller in intensity.[53] The two largest peaks at 3075 and 2977 cm^{-1} correspond to the CH_2 and CH_2 + CH stretching modes, respectively.[48,53] Other notable features in this stretching region are peaks at 2939 and 2964 cm^{-1} assigned to CH_3 stretching[46,49] and a peak at 3009 cm^{-1} assigned to CH stretching.[48]

Following 1×10^{18} atoms cm^{-2} of oxygen exposure, the aforementioned propene peaks change dramatically, many of them decaying in intensity. At the same time, there is significant growth of novel features that represent oxygenated products. Most notably in the solid line in Figure 1a, the spectral signature at 830 cm^{-1} is assigned to the ring deformation mode of propylene oxide (δ_{C2O}).[54−57] New peaks (1730 and 1693 cm^{-1}) in Figure 1b are similarly assigned to the C=O stretching frequency of propanal ($\nu_{C=O}$).[58−60] Additionally, there is a small amount of acetone produced, confirmed spectroscopically by the growth of a new peak at 1709 cm^{-1}, corresponding to its C=O stretching mode.[61,62]

In order to determine the role of film thickness in product formation and oxidative reactivity, propene films of increasing thickness ranging from 12 to 66 layers were dosed at 59 K and exposed to $O(^3P)$ at 54 K. Figure 2 depicts the decrease in the integrated area of the γ_w peak as propene films of varying

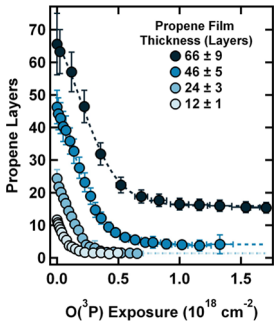

Figure 2. Changes in the number of propene layers on the surface (as determined via the integrated area of the $=CH_2$ wagging mode, γ_w) when films of varying thicknesses are exposed to $O(^3P)$ at 54 K demonstrate initial reactivity that slows upon extended exposure. $O(^3P)$ is only able to fully react with the film when the initial film has 24 layers of propene or fewer. Dotted lines are drawn to guide the eye.

thicknesses are exposed to $O(^3P)$. There is a clear period of initial linear reactivity for all films with a rate that is independent of the starting thickness. From these initial reactivity measurements, we estimate that ∼1 propene molecule reacts for every 100 oxygen atoms reaching the film surface. Given the observed rate of reaction and calculated barriers (below), this low reaction probability is perhaps surprising. We estimate, however, that at our surface temperatures, the sticking probability of oxygen atoms is on the order of 20% or less. This estimate was performed using the basic King and Wells technique[63] and thus explains why every oxygen atom reaching the film is not able to react with the propene film. Figure 2 also shows that after this initial period of exposure, there is a stark drop in reactivity. In the 12- and 24-layer films, the reaction tails off because oxygen reacts with propene completely down to the Au(111) substrate. In thicker films, however, oxygen is unable to fully react with propene in more buried layers. Moreover, the total reacted depth is inconsistent for both the 46- and 66-layer films (reaction complete at 4 layers and 23 layers remaining, respectively). This suggests that oxygen reactivity is connected to initial propene film thickness and that the reaction does not progress by simple layer-by-layer consumption of propene.

These results indicate that for films less than 70 layers thick (Figure 2), the initial reactivity of $O(^3P)$ + propene is linear and independent of film thickness. However, when examining thicker propene films (70−240 layers), the initial linear rate slows slightly (Figure 3a). When plotting the initial rates as a function of propene film thickness in layers, we see that the initial propene reactivity plateaus for films greater than 150 layers (Figure 3b). We note that frequencies of the γ_w mode do not shift upon increased propene deposition, confirming that there are no major changes in film structure or optical effects as coverage increases.[64] Rather, we propose that these changes in initial reaction rates can be attributed to increased barriers for oxygen diffusion within the film, as discussed in the Effect of Surface Temperature section.

Throughout oxygen exposure, propene disappearance is coupled to the growth of new spectral features corresponding to propylene oxide, propanal, and a small amount of acetone (Figure 1). Product growth is immediately observed upon $O(^3P)$ exposure by monitoring the integrated areas of

https://dx.doi.org/10.1021/acs.jpcc.9b11439
J. Phys. Chem. C XXXX, XXX, XXX−XXX

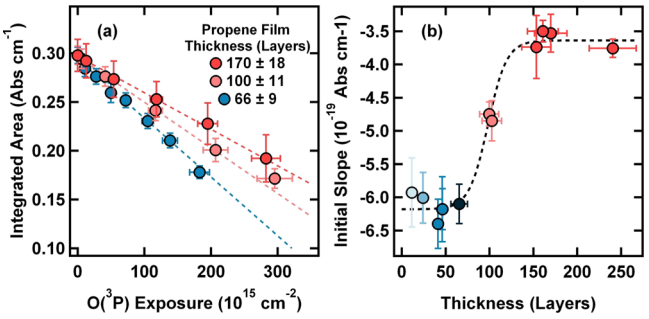

Figure 3. Integrated areas of the γ_w peak corresponding to 66-, 100-, and 170-layer thick propene films (a) show that the initial O(^{3}P) reactivity is linear with rates that depend on thickness. Taking these initial rates from (a) and including rates for films up to 240 layers (b) demonstrate that this initial rate slows for films greater than 70 layers but reaches a steady value for films greater than 150 layers. Dotted line in (b) is drawn to guide the eye.

propylene oxide's δ_{C2O} mode (Figure 4a) and propanal's $\nu_{C=O}$ mode (Figure 4b). We see that not only is there more

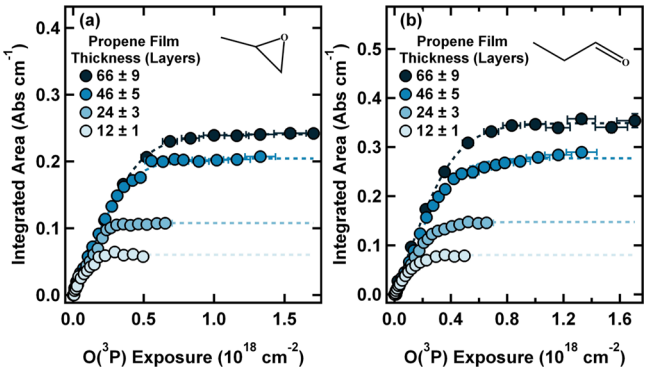

Figure 4. Integrated area of the propylene oxide ring deformation peak (δ_{C2O}, a) and propanal C═O peak ($\nu_{C=O}$, b) for propene films of varying thicknesses exposed to O(^{3}P) at 54 K demonstrates the growth of primary products with a similar linear rate. More products are formed in reactions with thicker films. Dotted lines are drawn to guide the eye.

propylene oxide and propanal formed in thicker films, but that the rate of formation of these products does not change with increasing film thickness (up to 70 MLs). During exposure at 54 K, the Au(111) substrate temperature is such that propene and our products (propanal and propylene oxide) are stable on the surface.[30,52,60] Even though our film composition changes (decrease in propene and increase in propanal and propylene oxide), there is limited desorption of products, and thus, our overall film thickness is likely comparable throughout. We detect no distortion or shifting of RAIR peaks as exposure continues and products form. Additionally, we expect that the index of refraction is comparable for alkene ices and oxygen hydrocarbons,[65] so we primarily attribute changes in peak intensity to reactivity and possibly molecular orientation, rather than optical effects as our films are likely less than 100 nm thick.[66]

In addition to RAIRS, temperature-programmed desorption (TPD) data can help to confirm product identities and their relative stabilities on the surface (Figure 5). For the 46-layer film, O(^{3}P) is unable to fully react with the film down to the substrate (Figure 2), and there are correspondingly low-

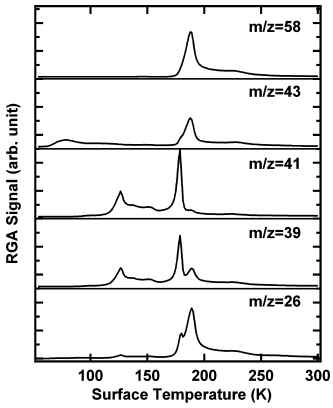

Figure 5. TPD of a 46-layer propene film after exposure to ~1 × 10^{18} atoms cm^{-2} of O(^{3}P) confirms the presence of propanal (m/z = 26, 58), propylene oxide (m/z = 26, 43, 58), and acetone (m/z = 43, 58). There is also some propene left on the surface (m/z = 39, 41).

temperature desorption features for propene at m/z = 39 and 41. As shown in Figure 5, these first desorption features peak at 119 K, closely matching previous studies for propene on Au(111).[52] Although it is difficult to quantitatively differentiate our products because of significantly overlapping cracking patterns, we can assign m/z = 43 to acetone and propylene oxide, m/z = 26 to propanal and propylene oxide, and m/z = 58 to propanal, propylene oxide, and acetone. As shown in Figure 5, acetone appears to be the least stable with a small desorption feature at 78 K, while propanal and propylene oxide have major desorption features at 175 K.[60,67] From this analysis, it is clear that propanal and propylene oxide are our major products in the condensed phase, which are more stable on the surface. It is possible that these products are in weakly bound multilayer films, while there is less than a ML of acetone.[62] We also note that we do not identify any high-molecular-weight polymeric or oligomeric species, which suggests that our intermediate product species are not long-lived on the surface.

Effect of Surface Temperature. In addition to characterizing film reactivity and product formation, we can use the initial reaction rates at surface temperatures ranging from 44 to 59 K to calculate the activation energy for the disappearance of propene (films of ~30 layers thick). The ═CH_2 wagging mode of propene (γ_w) is composed of two features at 919 and 914 cm^{-1} (Figure 1). Upon exposure to O(^{3}P), Figure 6a

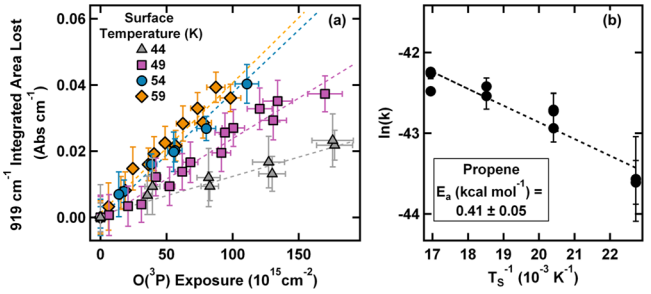

Figure 6. Integrated area lost from the 919 cm^{-1} peak (part of the ═CH_2 wagging mode, γ_w) corresponding to ~30-layer thick propene films exposed to O(^{3}P) (a) provides initial linear reaction rates for surface temperatures ranging from 44 to 59 K. These rates are fit to an Arrhenius model (b), giving an experimental activation energy of 0.41 ± 0.05 kcal mol^{-1}.

https://dx.doi.org/10.1021/acs.jpcc.9b11439
J. Phys. Chem. C XXXX, XXX, XXX−XXX

depicts the loss of integrated area of 919 cm^{-1} peak for four different surface temperatures (all films dosed at 59 K). A corresponding Arrhenius plot is shown in Figure 6b; the calculated activation energy for the removal of propene's double bond is 0.41 ± 0.05 kcal mol^{-1}. Under our experimental conditions, this activation energy is similar to or less than those reported in gas-phase studies of the same system.[68−70] However, because this value is calculated simply from the disappearance of propene, it is possibly a convolution of three different reaction steps, each of which will be explored in detail below.

The first challenge hidden within the measured activation energy is a question of product formation and reaction mechanism. The observed product distribution for the $O(^3P)$ + propene reaction is well supported by a mechanism[71,72] (Figure 7) in which $O(^3P)$ attacks the double bond to form a

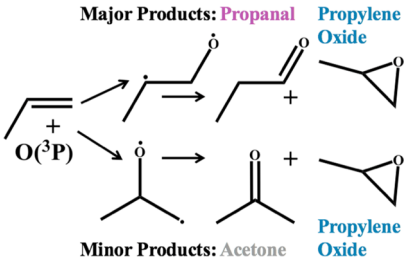

Figure 7. Reported mechanism for the $O(^3P)$ reaction with condensed propene: $O(^3P)$ is expected to preferentially attack the least substituted side of the double bond to form a triplet biradical intermediate that progresses, via ISC, to the final products propylene oxide and propanal.

triplet biradical intermediate. It is important to note that our reaction products (acetone, propanal, and propylene oxide) are singlet species. As outlined by the PES in Leonori et al.,[15] it is clear that our reaction proceeds almost 100% via ISC to the singlet surface, leading to our observed products. This can be accounted for by recent studies,[15,73] demonstrating that ISC and nonadiabatic effects become increasingly important as the reaction temperature decreases.[74]

As mentioned above, however, the measured activation energy for propene oxidation may include barrier contributions for oxygen addition to *either side* of the double bond (Figure 7). To parse these contributions, we perform the same Arrhenius analysis on product formation using the integrated area of propylene oxide's δ_{C2O} mode and propanal's $\nu_{C=O}$ mode as a function of $O(^3P)$ exposure. Propylene oxide is a major product in both addition channels, while propanal should only be formed from the addition of oxygen to the terminal propene carbon.

The results of this analysis show that the activation energy is 0.36 ± 0.03 kcal mol^{-1} for propylene oxide formation (Figure 8a) and 0.34 ± 0.06 kcal mol^{-1} for propanal formation (Figure 8b). These values are in good agreement with one another, and they are also within the error of the measured activation energy for the destruction of propene's double bond (0.41 ± 0.05 kcal mol^{-1}). This suggests that not only is oxygen addition to the terminal carbon the dominating pathway obeying Cvetanovic's rules for oxygen addition to alkenes,[71] but the addition step itself is rate-limiting.[18] This makes sense for our low-temperature, condensed phase environment given that in the gas phase the barrier for $O(^3P)$ addition is three times higher

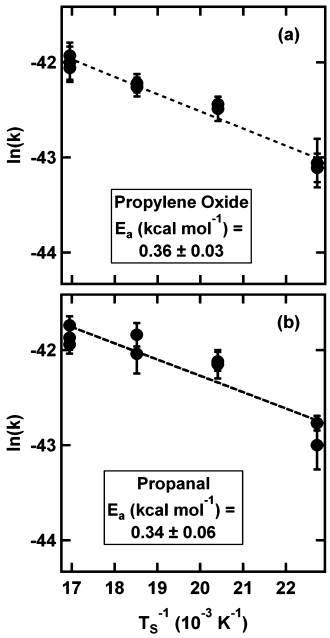

Figure 8. Initial rate constants of propylene oxide (a) and propanal (b) formation from ∼30-layer thick propene films exposed to $O(^3P)$ over temperatures ranging from 44 to 59 K are fit to an Arrhenius model. The experimental activation energies are 0.36 ± 0.03 and 0.34 ± 0.06 kcal mol^{-1} for propylene oxide and propanal formation, respectively.

for the central carbon compared to that for the terminal carbon.[15]

To further assess the mechanism, we examine changes in the CH region associated with the terminal and central carbons. This analysis is shown for a representative 46-layer film, but these trends are consistent for films of varying thicknesses. In particular, as shown in Figure 9a, we track changes in peaks at

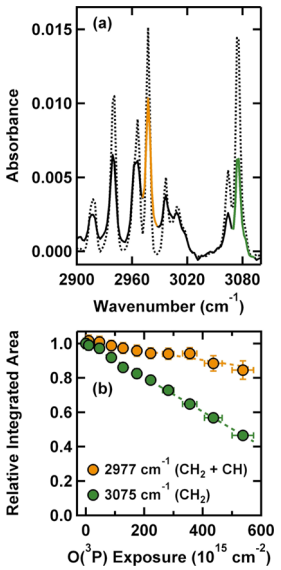

Figure 9. (a) RAIR spectra of the CH region of a 46-layer propene film before (dashed line) and after exposure to $O(^3P)$ (solid line, total exposure ≈ 5 × 10^{17} atoms cm^{-2}) at 54 K show significant reactivity. (b) Normalized intensities as a function of exposure demonstrate different rates of reaction for peaks at 2977 cm^{-1} (orange, CH_2 + CH stretching mode) and 3075 cm^{-1} (green, CH_2 stretching mode).

https://dx.doi.org/10.1021/acs.jpcc.9b11439
J. Phys. Chem. C XXXX, XXX, XXX−XXX

2977 cm^{-1} (CH_2 + CH stretching) and 3075 cm^{-1} (CH_2 stretching). We integrated these two peaks as a function of $O(^3P)$ exposure and normalized their intensity to the pristine film (Figure 9b). When oxygen atoms are introduced into the film, there is a clear decay in intensity for both peaks, again supporting that atomic oxygen is easily able to react with the condensed propene. The relative reaction rates in Figure 9b suggest that the reactivity is greater for the 3075 cm^{-1} peak corresponding to only CH_2 stretches (green) compared to the 2977 cm^{-1} peak corresponding to CH_2 + CH stretches (orange). This can be interpreted as again reinforcing that oxygen addition to the terminal carbon is the dominant pathway. We also note that because we are using RAIRS, this trend may also be linked to a change in average molecular orientation; this is, however, unlikely to be a significant contribution because of the thick, polycrystalline nature of the film.[47]

Also complicating this analysis is a small decrease in intensity of the peaks at 2939 cm^{-1} and 2964 cm^{-1} corresponding to the CH_3 stretching modes. This suggests that although oxygen addition is the dominant mechanism, hydrogen abstraction may be a minor secondary pathway. Gas-phase studies found that H abstraction was unable to compete with oxygen addition,[75] and although barriers in the condensed phase are often lower, we do not expect that H abstraction is a significant contribution to the overall reaction mechanism. H abstraction would necessarily yield a highly reactive hydroxyl radical,[3] which we see no evidence for in our product analysis. Moreover, abstraction leaves behind a carbon-centered radical that could easily continue to react with other molecules in the film or with oxygen species in the beam. It is possible that a small amount of acrolein is formed through this channel, but it is certainly only a minor contribution.

The second challenge with quantifying a reaction barrier for this system in the condensed phase is the potential contribution of oxygen diffusion. To untangle this contribution, we return to the difference in initial reaction rates observed between thin (<70 layer) and thick (>150 layer) films. By performing the same Arrhenius analysis again on 150 ML films, we find that the activation energy for the reaction of propene's double bond is 1.06 ± 0.11 kcal mol^{-1}. This is significantly higher than the calculated barrier for ∼30-layer propene films (0.41 kcal mol^{-1}), suggesting that oxygen diffusion through the film plays a significant role in the observed reaction in thicker films.[71,76−78] The thinnest propene films (<70 layers) may contain more small defects, grain boundaries, and islands that provide oxygen more access to the bulk. In other words, the reaction is not diffusion-controlled for thin films because there is less need for diffusion: the surface is likely inhomogeneous with exposed propene islands.[79] Higher reactivity at defects and grain boundaries is well documented,[80,81] and as with other thick molecular films, self-similarity may not be achieved until a certain thickness is reached (often >100 layers).[82−85] Our results, therefore, suggest that propene films reach self-similarity at approximately 150 layers, at which point oxygen diffusion becomes limiting.

Effect of the Propene Film Structure. For all experiments mentioned so far, propene films were deposited at a surface temperature of 59 K and exposed to oxygen at temperatures between 44 and 59 K. However, as shown in Figure 10, the deposition substrate temperature has a profound impact on the RAIR spectra of the pristine propene film,

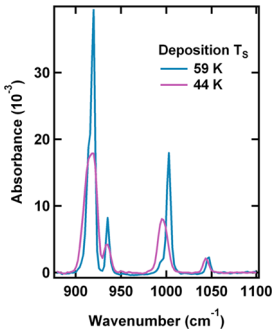

Figure 10. RAIR spectra of characteristic regions of 46-layer condensed propene films demonstrate that films deposited at 44 K (pink) are significantly different from the films deposited at 59 K (blue). The peaks corresponding to the γ_w mode, the C═C wagging mode, the CH_2 twisting + CH out-of-plane bending mode, and the CH_3 rock + CH out-of-plane mode in the low-temperature film are generally broader and red-shifted from the analogous high-temperature film. Such shifts indicate a more disordered and amorphous film.

indicating a significant difference in film morphology. This is true regardless of film thickness. The spectral differences between a propene film produced at 59 K and that produced at 44 K can be summarized as follows: the γ_w peak broadens and red-shifts by 2 cm^{-1} to 918 cm^{-1}, the C═C wagging mode red-shifts by 2 cm^{-1} to 933 cm^{-1}, the CH_2 twisting + CH out-of-plane bending mode red-shifts by 7 cm^{-1} to 995 cm^{-1}, and the CH_3 rock + CH out-of-plane bending mode red-shifts by 4 cm^{-1} to 1043 cm^{-1}. These alkene modes are known to be sensitive to the conformation of the molecule and local changes within the environment.[86] In general, the peak shifts and broadening observed for the propene film dosed at 44 K compared to the propene film at 59 K are attributed to increased film disorder.[46,52,87] Red shifts may also be a result of increased intermolecular interactions with surrounding propene molecules, resulting in a slight weakening of the ═CH_2 bond.

Although this is, to our knowledge, the first spectral evidence of differing morphologies of condensed propene, it is not unusual for deposition conditions to influence mobility during film deposition, leading to different film phases at different temperatures and dosing rates. There is a vast literature, for example, on the growth of amorphous solid water and crystalline water ice films whereby crystalline films are only possible at higher substrate temperatures where there is enough mobility for water molecules to rearrange during dosing or upon annealing.[82,88−90] Similarly for alkenes, amorphous acetylene (produced at 12 K) and crystalline acetylene (produced at 70 K) have been clearly identified spectroscopically.[91] Upon warming the amorphous acetylene from 12 K, an irreversible change was detected in the spectra between 40 and 50 K, indicating that the amorphous acetylene ice had crystallized. Such spectral changes between amorphous and crystalline films have also been detected for ethane and ethylene;[65] warming films to 60 K always resulted in crystallization. Based on the similarities between our observations and these studies, we will use the terms "amorphous" and "crystalline" to differentiate the films deposited below 44 or at 59 K, respectively, as propene films are less ordered when deposited below 44 K and more highly ordered at 59 K.

In order to determine how the propene structure impacts oxidative reactivity, a crystalline film dosed at 59 K and an

https://dx.doi.org/10.1021/acs.jpcc.9b11439
J. Phys. Chem. C XXXX, XXX, XXX−XXX

amorphous film dosed at 44 K were exposed to O(^{3}P) at an intermediate temperature of 49 K (Figure 11). At 49 K, both

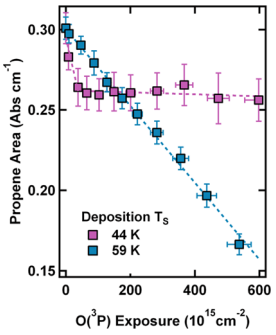

Figure 11. Changes in the integrated area of the γ_w mode for a 46-layer propene film dosed at 44 K (pink) and 59 K (blue) and exposed to O(^{3}P) at 49 K demonstrate that while films dosed at 44 K do experience some initial reactivity, O(^{3}P) is unable to penetrate into the bulk of the film; diffusion and reaction occur more readily for propene films deposited at 59 K.

propene films remain structurally the same when deposited, that is, the amorphous film is unable to irreversibly change to a crystalline structure and vice versa. As expected, the reaction rate for the crystalline film (blue) is linear as oxygen reacts with the film. On the other hand, the amorphous film grown at 44 K is largely unreactive. There is a very short initial period of reactivity, which we attribute to O(^{3}P) reacting with the disordered propene surface layers at the vacuum interface. After this, however, there is little to no reaction despite extended exposure; this is true for all RAIR spectral regions, including CH. It is interesting to note that the initial reaction rate of the amorphous film is faster than the rate of the crystalline film. This may further support the "amorphous" versus "crystalline" designation of the two films. A more amorphous film typically presents a larger exposed surface area (due to islands, microporous pockets, and undercoordinated surface molecules) than the crystalline film.[92,93] A larger surface area would provide more accessible surface propene molecules, and thus, a faster observable rate of initial reaction before oxygen penetration into the bulk becomes necessary for continued reaction.

Beyond the first seconds of reactivity, it is quite surprising that the reactivity plateaus drastically for the amorphous film. These results suggest that oxygen is unable to diffuse into the propene bulk when the film has a more amorphous structure. This behavior is supported by previous studies examining the oxidative reactivity of self-assembled MLs,[94−96] where it has been found that a more compact and less mobile film structure was not as reactive. Additionally, it has been suggested that film density plays a role in observed spectroscopic band strengths, as is the case for amorphous methane.[97] Thus, the lower intensity of the peaks corresponding to amorphous propene could indicate increased density compared to the crystalline propene film. Although larger diffusion barriers in amorphous films are less common, there are polymer films where the amorphous regions are denser, and this trend has been observed.[98,99] This suggests that our amorphous propene film may be packed more closely, making it less accessible to the permeating oxygen. We know from previous studies that ML propene molecules organize with the double bond nearly parallel to the Au(111) substrate.[52] This molecular orientation also appears to propagate to thicker multilayer crystalline propene films as well.[46] Thus, it is possible that in this crystalline propene structure, the molecules are organized in such a way that intermolecular spacing affords easy access for oxygen to diffuse into the film and encounter propene's double bond.[100] It is also likely that our propene films are polycrystalline and that grain boundaries further facilitate diffusion.[94]

RAIR spectra of the amorphous and crystalline forms of propene are easily differentiated, allowing us to probe the amorphous to crystallization transition directly and extract an activation energy for the process. Amorphous propene films (70-layer thick) were dosed at 44 K and subjected to isothermal annealing at 50, 51, 51.5, 52, 53, 54, and 55 K. Spectra collected every 60−90 s during the annealing clearly demonstrate a sharp phase transition (Figure 12a), evidenced

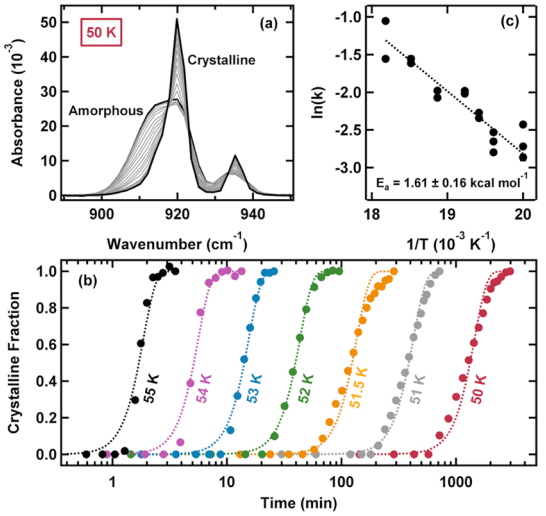

Figure 12. (a) Time-resolved RAIR spectra of a 70-layer propene film isothermally annealed at 50 K indicate a transition from amorphous to crystalline propene. (b) Representative crystalline fractions vs annealing time are fit to the Avrami equation (eq 1, dashed lines) using k as a fit parameter and a n value of 4 (see the text for details). Crystalline fractions are established using the relative intensities of the corresponding spectra at 919 cm^{-1}. (c) Rate constants (k) are fit to an Arrhenius equation, yielding an activation of 1.61 ± 0.16 kcal mol^{-1} for the crystallization of propene.

by a sharpening of the peak at 919 cm^{-1} and a decrease in relative intensity of the 914 cm^{-1} shoulder. The crystallization process occurs over a time scale of 5−30 min depending on the temperature.

Rate constants for the crystallization were established by tracking the change in intensity at 919 cm^{-1} throughout the annealing. As shown in Figure 12a, the crystallizing spectra have multiple isosbestic points where the spectra overlap, indicating a linear combination of crystalline and amorphous states.[101] Thus, the relative intensity of this point to both the starting fully amorphous film and the ending fully crystalline film can be used to establish the crystalline fraction of the film at any point of time.

This analysis is shown for a representative trial at each temperature by the dotted data in Figure 12b. The corresponding fit (illustrated by a dashed line) is the integrated form of the Avrami[102−104] equation

https://dx.doi.org/10.1021/acs.jpcc.9b11439
J. Phys. Chem. C XXXX, XXX, XXX−XXX

$$x(t) = 1 - e^{-(kt)^n} \quad (1)$$

This form of the Avrami equation is commonly used to describe phase transformation by nucleation and gives the crystallized fraction of a material ($x(t)$) as a function of time during isothermal annealing. In eq 1, k is the crystallization rate constant (experimental fit parameter) and n is a parameter related to the crystallization mechanism.[101] A value of $n = 4$ fits the data well, suggesting that the nucleation rate is constant and that there is isotropic three-dimensional growth of the crystalline phase.[105,106] We note, however, that the value of n has little impact on the calculated activation energy for propene crystallization, which is the focus of this analysis.

An activation energy for the crystallization was calculated by assuming that the crystallization rate constants have an Arrhenius-like temperature dependence. This plot is shown in Figure 12c; the corresponding analysis gives an activation energy of 1.61 ± 0.16 kcal mol^{-1}. This activation energy is much lower than those reported for water[101] or methanol[107] ices (~17−23 kcal mol^{-1}), indicating a low barrier for this irreversible change to crystalline propene. One possible explanation for this low value is that our amorphous propene is in a metastable state, similar to that observed in ethane, ethylene, and acetylene ices.[65,91] Even though we do not observe any additional spectral differences between propene deposited between 20 and 44 K, amorphous solid water ices are known to be metastable compared to crystalline ices.[108] A second explanation for the difference may be that the propene films used are thin (~70-layers); water film crystallization kinetics, for example, are only independent of thickness for films greater than 300 layers.[109]

Regardless, this analysis highlights a number of interesting features of the propene system. First, the Avrami fitting procedure and low activation energy barrier suggest that crystallization occurs rapidly, with nucleation occurring randomly (i.e., the weak physisorption interaction between propene and the Au(111) substrate is not the dominating factor in crystallization nucleation). Additionally, we demonstrate the general feasibility of using isothermal annealing and corresponding spectra to determine alkene crystalline activation energies, which can be useful in discussing the relative stabilities of solids, liquids, and supercooled liquids.[107]

The discovery of multiple propene phases may also help to explain the observations from Figure 2, in which O(^{3}P) is unable to fully erode thicker films and the total reacted depth is inconsistent among thicker films. When propene films crystallize (Figure 12a), RAIR spectra show a dramatic change in the relative intensity of the γ_w mode; the 914 cm^{-1} shoulder decreases in intensity, while the 919 cm^{-1} peak increases. During oxidation, this bluer peak (919 cm^{-1}) is consumed more readily (Figure 13). This may indicate that within "crystalline" films, there is no uniform O(^{3}P) reactivity within the film. Instead, it is possible that because of inhomogeneity in film organization, there are certain domains of increased order or accessibility where oxygen diffusion and reaction occur more readily. Our results, therefore, show broadly that the film structure can have a dramatic impact on observed reactivity by impeding or allowing efficient reactant diffusion.

CONCLUSIONS

The oxidative reactivity of condensed propene films at cryogenic surface temperatures has been characterized using time-resolved RAIRS. We find that in the condensed phase,

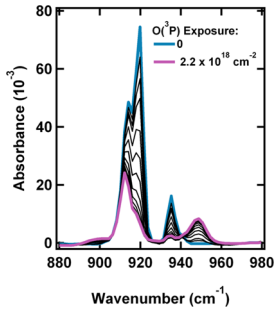

Figure 13. Upon exposure to O(^{3}P), RAIR spectra of the γ_w propene mode show a faster rate of intensity decrease for the higher wavenumber peak (919 cm^{-1}), indicating that there may be multiple domains within the propene film and that some of them are more accessible to O(^{3}P) reactivity.

propene reacts readily with O(^{3}P) to form primarily propylene oxide and propanal, supporting a mechanism where oxygen almost always preferentially adds to the least substituted side of the double bond. Following addition, the triplet biradical intermediate undergoes ISC at a likelihood of close to 100% to form the singlet products: propanal, propylene oxide, and a small amount of acetone. The activation energy for the loss of propene in the O(^{3}P) + propene reaction for ~30-layer thick films is 0.41 ± 0.05 kcal mol^{-1}, while the activation energy is 0.36 ± 0.03 for propylene oxide formation and 0.34 ± 0.06 kcal mol^{-1} for propanal formation. When examining thicker films (150 MLs), we find that the activation energy for the reaction of propene's double bond is 1.06 ± 0.11 kcal mol^{-1}, which suggests that oxygen diffusion through the film plays a significant role in the observed reaction. Interestingly, it is possible to spectroscopically differentiate two forms of propene: an amorphous form present at lower deposition temperatures (<44 K) and a crystalline form present at 59 K. Little reactivity is observed when the propene film is more disordered. Additionally, because RAIR spectra of the amorphous and crystalline forms of propene are easily differentiated, it is possible to probe the amorphous to crystallization transition directly and extract an activation energy for this process.

Overall, this work provides fundamental mechanistic insights into the diffusion and reactivity of ground-state atomic oxygen in condensed films of small, unsaturated hydrocarbons. Our results indicate that despite low reaction barriers for oxygen diffusion, film composition and morphology can have a significant impact on reactant diffusion and subsequent reactivity. In general, such work informs the development of novel industrial processes used in the production of polyurethane plastics as well as sheds light on possible chemical pathways in frozen astrophysical environments. In addition to these applications, an important future extension of this work may be to consider conformationally ordered, vinyl-containing films in which molecular orientation relative to the impinging oxygen atom can be controlled, allowing for precise, stereodynamic tuning of reaction kinetics.

AUTHOR INFORMATION

Corresponding Author

S. J. Sibener − *The James Franck Institute and Department of Chemistry, The University of Chicago, Chicago, Illinois 60637, United States;* orcid.org/0000-0002-5298-5484; Email: s-sibener@uchicago.edu

https://dx.doi.org/10.1021/acs.jpcc.9b11439
J. Phys. Chem. C XXXX, XXX, XXX−XXX

Authors

Michelle R. Brann − *The James Franck Institute and Department of Chemistry, The University of Chicago, Chicago, Illinois 60637, United States*

Rebecca S. Thompson − *The James Franck Institute and Department of Chemistry, The University of Chicago, Chicago, Illinois 60637, United States*

Complete contact information is available at: https://pubs.acs.org/10.1021/acs.jpcc.9b11439

Notes

The authors declare no competing financial interest.

■ ACKNOWLEDGMENTS

This work was supported by the National Science Foundation, grant no. CHE-1900188. Additional support was provided by the NSF-Materials Research Science and Engineering Center at The University of Chicago, grant no. NSF-DMR-14-20709.

■ REFERENCES

(1) Davis, S. G.; Law, C. K.; Wang, H. Propene Pyrolysis and Oxidation Kinetics in a Flow Reactor and Laminar Flames. *Combust. Flame* **1999**, *119*, 375−399.

(2) Lissianski, V. V.; Zamansky, V. M.; Gardiner, W. C. Combustion Chemistry Modeling. In *Gas-Phase Combustion Chemistry*; Gardiner, W. C., Ed.; Springer, 2000; pp 1−123.

(3) Nguyen, T. L.; Peeters, J.; Vereecken, L. Quantum Chemical and Statistical Rate Study of the Reaction of $O(^3P)$ with Allene: O-Addition and H-Abstraction Channels. *J. Phys. Chem. A* **2006**, *110*, 12166−12176.

(4) Lambert, R. M.; Williams, F. J.; Cropley, R. L.; Palermo, A. Heterogeneous Alkene Epoxidation: Past, Present and Future. *J. Mol. Catal. A Chem.* **2005**, *228*, 27−33.

(5) Kahlich, D.; Wiechern, U.; Linder, J. Propylene Oxide. In *Ullmann's Encyclopedia of Industrial Chemistry*; Wiley, 2012; Vol. *30*, pp 313−335.

(6) Kirschner, E. M. Production of Top 50 Chemicals Increased Substantially in 1994. *Chem. Eng. News* **1995**, *73*, 16−20.

(7) Manz, T. A.; Yang, B. Selective Oxidation Passing through η^3-Ozone Intermediates: Applications to Direct Propene Epoxidation Using Molecular Oxygen Oxidant. *RSC Adv.* **2014**, *4*, 27755−27774.

(8) Cavani, F. Catalytic Selective Oxidation: The Forefront in the Challenge for a More Sustainable Chemical Industry. *Catal. Today* **2010**, *157*, 8−15.

(9) Lee, H.-J.; Shi, T.-P.; Busch, D. H.; Subramaniam, B. A Greener, Pressure Intensified Propylene Epoxidation Process with Facile Product Separation. *Chem. Eng. Sci.* **2007**, *62*, 7282−7289.

(10) Koda, S.; Endo, Y.; Tsuchiya, S.; Hirota, E. Branching Ratios in $O(^3P)$ Reactions of Terminal Olefins Studied by Kinetic Microwave Absorption Spectroscopy. *J. Phys. Chem.* **1991**, *95*, 1241−1244.

(11) Quandt, R.; Min, Z.; Wang, X.; Bersohn, R. Reactions of $O(^3P)$ with Alkenes: H, CH_2CHO, CO, and OH Channels. *J. Phys. Chem. A* **1998**, *102*, 60−64.

(12) Savee, J. D.; Welz, O.; Taatjes, C. A.; Osborn, D. L. New Mechanistic Insights to the $O(^3P)$ + Propene Reaction from Multiplexed Photoionization Mass Spectrometry. *Phys. Chem. Chem. Phys.* **2012**, *14*, 10410−10423.

(13) Cvetanović, R. J. Addition of Atoms to Olefins in the Gas Phase. In *Advances in Photochemistry*; John Wiley & Sons, Ltd, 1963; pp 115−182.

(14) Morin, J.; Bedjanian, Y.; Romanias, M. N. Rate Constants of the Reactions of $O(^3P)$ Atoms with Ethene and Propene over the Temperature Range 230-900 K. *Int. J. Chem. Kinet.* **2017**, *49*, 53−60.

(15) Leonori, F.; Balucani, N.; Nevrly, V.; Bergeat, A.; Falcinelli, S.; Vanuzzo, G.; Casavecchia, P.; Cavallotti, C. Experimental and Theoretical Studies on the Dynamics of the $O(^3P)$ + Propene Reaction: Primary Products, Branching Ratios, and Role of Intersystem Crossing. *J. Phys. Chem. C* **2015**, *119*, 14632−14652.

(16) Cavallotti, C.; Leonori, F.; Balucani, N.; Nevrly, V.; Bergeat, A.; Falcinelli, S.; Vanuzzo, G.; Casavecchia, P. Relevance of the Channel Leading to Formaldehyde + Triplet Ethylidene in the $O(^3P)$ + Propene Reaction under Combustion Conditions. *J. Phys. Chem. Lett.* **2014**, *5*, 4213−4218.

(17) Hughes, A. N.; Scheer, M. D.; Klein, R. The Reaction between $O(^3P)$ and Condensed Olefins below 100 K. *J. Phys. Chem.* **1966**, *70*, 798−805.

(18) Klein, R.; Scheer, M. D. Mechanism of $O(^3P)$ Addition to Condensed Films. II. Propene, 1-Butene, and Their Mixtures. *J. Phys. Chem.* **1968**, *72*, 617−622.

(19) Cvetanović, R. J. Mechanism of the Interaction of Oxygen Atoms with Olefins. *J. Chem. Phys.* **1956**, *25*, 376−377.

(20) Atkinson, R.; Cvetanović, R. J. Activation Energies of the Addition of $O(^3P)$ Atoms to Olefins. *J. Chem. Phys.* **1972**, *56*, 432−437.

(21) Ward, M. D.; Price, S. D. Thermal Reactions of Oxygen Atoms with Alkenes at Low Temperatures on Interstellar Dust. *Astrophys. J.* **2011**, *741*, 121.

(22) Burke, D. J.; Brown, W. A. Ice in Space: Surface Science Investigations of the Thermal Desorption of Model Interstellar Ices on Dust Grain Analogue Surfaces. *Phys. Chem. Chem. Phys.* **2010**, *12*, 5947−5969.

(23) Herbst, E. Chemistry in the Interstellar Medium. *Annu. Rev. Phys. Chem.* **1995**, *46*, 27−54.

(24) Hickson, K. M.; Wakelam, V.; Loison, J.-C. Methylacetylene (CH_3CCH) and Propene (C_3H_6) Formation in Cold Dense Clouds: A Case of Dust Grain Chemistry. *Mol. Astrophys.* **2016**, *3*−*4*, 1−9.

(25) Marcelino, N.; Cernicharo, J.; Agúndez, M.; Roueff, E.; Gerin, M.; Martín-Pintado, J.; Mauersberger, R.; Thum, C. Discovery of Interstellar Propylene (CH_2CHCH_3): Missing Links in Interstellar Gas-Phase Chemistry. *Astrophys. J.* **2007**, *665*, L127−L130.

(26) Nixon, C. A.; Jennings, D. E.; Bézard, B.; Vinatier, S.; Teanby, N. A.; Sung, K.; Ansty, T. M.; Irwin, P. G. J.; Gorius, N.; Cottini, V.; et al. Detection of Propene in Titan's Stratosphere. *Astrophys. J.* **2013**, *776*, L14.

(27) Rawlings, J. M. C.; Williams, D. A.; Viti, S.; Cecchi-Pestellini, C. A Radical Route to Interstellar Propylene Formation. *Mon. Not. R. Astron. Soc. Lett.* **2013**, *436*, L59−L63.

(28) Garrod, R. T.; Wakelam, V.; Herbst, E. Non-Thermal Desorption from Interstellar Dust Grains via Exothermic Surface Reactions. *Astron. Astrophys.* **2007**, *467*, 1103−1115.

(29) McGuire, B. A.; Carroll, P. B.; Loomis, R. A.; Finneran, I. A.; Jewell, P. R.; Remijan, A. J.; Blake, G. A. Discovery of the Interstellar Chiral Molecule Propylene Oxide (CH_3CHCH_2O). *Science* **2016**, *352*, 1449−1452.

(30) Bergantini, A.; Abplanalp, M. J.; Pokhilko, P.; Krylov, A. I.; Shingledecker, C. N.; Herbst, E.; Kaiser, R. I. A Combined Experimental and Theoretical Study on the Formation of Interstellar Propylene Oxide (CH_3CHCH_2O)—A Chiral Molecule. *Astrophys. J.* **2018**, *860*, 108.

(31) Bergner, J. B.; Öberg, K. I.; Rajappan, M. Methanol Formation via Oxygen Insertion Chemistry in Ices. *Astrophys. J.* **2017**, *845*, 29.

(32) Bergner, J. B.; Öberg, K. I.; Rajappan, M. Oxygen Atom Reactions with C_2H_6, C_2H_4, and C_2H_2 in Ices. *Astrophys. J.* **2019**, *874*, 115.

(33) Gibson, K. D.; Killelea, D. R.; Yuan, H.; Becker, J. S.; Sibener, S. J. Determination of the Sticking Coefficient and Scattering Dynamics of Water on Ice Using Molecular Beam Techniques. *J. Chem. Phys.* **2011**, *134*, 034703.

(34) Callen, B. W.; Griffiths, K.; Memmert, U.; Harrington, D. A.; Bushby, S. J.; Norton, P. R. The Adsorption of Water on Ni(110): Monolayer, Bilayer and Related Phenomena. *Surf. Sci.* **1990**, *230*, 159−174.

(35) Nakao, F. Determination of the Ionization Gauge Sensitivity Using the Relative Ionization Cross-Section. *Vacuum* **1975**, *25*, 431−435.

(36) Itikawa, Y. Cross Sections for Electron Collisions with Nitrogen Molecules. *J. Phys. Chem. Ref. Data* **2006**, *35*, 31−53.
(37) Stein, S. E. Infrared Spectra. In *NIST Chemistry WebBook, NIST Standard Reference Database Number 69*; Linstrom, P. J., Mallard, W. G., Eds.; NIST standard reference database; National Institute of Standards and Technology: Gaithersburg MD, 2018.
(38) Sharpe, S. W.; Johnson, T. J.; Sams, R. L.; Chu, P. M.; Rhoderick, G. C.; Johnson, P. A. Gas-Phase Databases for Quantitative Infrared Spectroscopy. *Appl. Spectrosc.* **2004**, *58*, 1452−1461.
(39) Es-sebbar, E.-t.; Alrefae, M.; Farooq, A. Infrared Cross-Sections and Integrated Band Intensities of Propylene: Temperature-Dependent Studies. *J. Quant. Spectrosc. Radiat. Transf.* **2014**, *133*, 559−569.
(40) Sung, K.; Toon, G. C.; Drouin, B. J.; Mantz, A. W.; Smith, M. A. H. FT-IR Measurements of Cold Propene (C_3H_6) Cross-Sections at Temperatures between 150 and 299 K. *J. Quant. Spectrosc. Radiat. Transf.* **2018**, *213*, 119−132.
(41) Sibener, S. J.; Buss, R. J.; Ng, C. Y.; Lee, Y. T. Development of a Supersonic O(^3P_J), O($^1D_2$) Atomic Oxygen Nozzle Beam Source. *Rev. Sci. Instrum.* **1980**, *51*, 167−182.
(42) Alagia, M.; Aquilanti, V.; Ascenzi, D.; Balucani, N.; Cappelletti, D.; Cartechini, L.; Casavecchia, P.; Pirani, F.; Sanchini, G.; Volpi, G. G. Magnetic Analysis of Supersonic Beams of Atomic Oxygen, Nitrogen, and Chlorine Generated from a Radio-Frequency Discharge. *Isr. J. Chem.* **1997**, *37*, 329−342.
(43) Casavecchia, P.; Balucani, N.; Volpi, G. G. Reactive Scattering of O(^{3}P, ^{1}D), Cl(^{2}P) and OH Radicals. In *The Chemical Dynamics and Kinetics of Small Radicals*; Wagner, A., Liu, K., Eds.; World Scientific Publishing Company, 1996; pp 365−426.
(44) Itikawa, Y. Cross Sections for Electron Collisions with Oxygen Molecules. *J. Phys. Chem. Ref. Data* **2009**, *38*, 1−20.
(45) Garton, D. J.; Minton, T. K.; Alagia, M.; Balucani, N.; Casavecchia, P.; Gualberto Volpi, G. Reactive Scattering of Ground-State and Electronically Excited Oxygen Atoms on a Liquid Hydrocarbon Surface. *Faraday Discuss.* **1997**, *108*, 387−399.
(46) Huang, W. X.; White, J. M. Propene adsorption on Ag(111): a TPD and RAIRS study. *Surf. Sci.* **2002**, *513*, 399−404.
(47) Chesters, M. A.; De La Cruz, C.; Gardner, P.; McCash, E. M.; Pudney, P.; Shahid, G.; Sheppard, N.; Sheppard, N. Infrared Spectroscopic Comparison of the Chemisorbed Species from Ethene, Propene, But-1-ene and *cis*- and *trans*-But-2-ene on Pt(111) and on a Platinum/Silica Catalyst. *J. Chem. Soc. Faraday Trans.* **1990**, *86*, 2757−2763.
(48) Radziszewski, J. G.; Downing, J. W.; Gudipati, M. S.; Balaji, V.; Thulstrup, E. W.; Michl, J. How Predictable Are IR Transition Moment Directions? Vibrational Transitions in Propene and Deuterated Propenes. *J. Am. Chem. Soc.* **1996**, *118*, 10275−10284.
(49) Barnes, A. J.; Howells, J. D. R. Infra-red cryogenic studies. Part 12.-Alkenes in argon matrices. *J. Chem. Soc., Faraday Trans. 2* **1973**, *69*, 532−539.
(50) Silvi, B.; Labarbe, P.; Perchard, J. P. Spectres de Vibration et Coordonnées Normales de Quatre Espèces Isotopiques de Propène. *Spectrochim. Acta Part A Mol. Spectrosc.* **1973**, *29*, 263−276.
(51) Huang, W. X.; White, J. M. Propene Oxidation on Ag(111): Spectroscopic Evidence of Facile Abstraction of Methyl Hydrogen. *Catal. Lett.* **2002**, *84*, 143−146.
(52) Davis, K. A.; Goodman, D. W. Propene Adsorption on Clean and Oxygen-Covered Au(111) and Au(100) Surfaces. *J. Phys. Chem. B* **2000**, *104*, 8557−8562.
(53) McKean, D. C. CH Stretching Frequencies, Bond Lengths and Strengths in Acetone, Acetaldehyde, Propene and Isobutene. *Spectrochim. Acta Part A Mol. Spectrosc.* **1975**, *31*, 861−870.
(54) Tobin, M. C. The Infrared Spectrum of Propylene Oxide. *Spectrochim. Acta* **1960**, *16*, 1108−1110.
(55) Brown, N. F.; Barteau, M. A. Epoxides as Probes of Oxametallacycle Chemistry on Rh(111). *Surf. Sci.* **1993**, *298*, 6−17.
(56) Stacchiola, D.; Burkholder, L.; Tysoe, W. T. Enantioselective Chemisorption on a Chirally Modified Surface in Ultrahigh Vacuum: Adsorption of Propylene Oxide on 2-Butoxide-Covered Palladium(111). *J. Am. Chem. Soc.* **2002**, *124*, 8984−8989.
(57) Dinger, A.; Lutterloh, C.; Biener, J.; Küppers, J. Adsorption of Propylene Oxide on Pt(111) Surfaces and Its Reactions with Gaseous and Adsorbed H Atoms. *Surf. Sci.* **2000**, *449*, 1−18.
(58) Davis, J. L.; Barteau, M. A. Polymerization and Decarbonylation Reactions of Aldehydes on the Pd(111) Surface. *J. Am. Chem. Soc.* **1989**, *111*, 1782−1792.
(59) Brown, N. F.; Barteau, M. A. Reactions of Unsaturated Oxygenates on Rhodium(111) as Probes of Multiple Coordination of Adsorbates. *J. Am. Chem. Soc.* **1992**, *114*, 4258−4265.
(60) Esan, D. A.; Trenary, M. Surface Chemistry of Propanal, 2-Propenol, and 1-Propanol on Ru(001). *Phys. Chem. Chem. Phys.* **2017**, *19*, 10870−10877.
(61) Vannice, M. A.; Erley, W.; Ibach, H. A RAIRS and HREELS Study of Acetone on Pt(111). *Surf. Sci.* **1991**, *254*, 1−11.
(62) Syomin, D.; Koel, B. E. IRAS studies of the orientation of acetone molecules in monolayer and multilayer films on Au() surfaces. *Surf. Sci.* **2002**, *498*, 53−60.
(63) King, D. A.; Wells, M. G. Molecular Beam Investigation of Adsorption Kinetics on Bulk Metal Targets: Nitrogen on Tungsten. *Surf. Sci.* **1972**, *29*, 454−482.
(64) Stacchiola, D.; Burkholder, L.; Tysoe, W. T. Structure and Reactivity of Propylene on Clean and Hydrogen-Covered Pd(111). *Surf. Sci.* **2003**, *542*, 129−141.
(65) Hudson, R. L.; Gerakines, P. A.; Moore, M. H. Infrared Spectra and Optical Constants of Astronomical Ices: II. Ethane and Ethylene. *Icarus* **2014**, *243*, 148−157.
(66) Mitlin, S.; Leung, K. T. Film Growth of Ice by Vapor Deposition at 128−185 K Studied by Fourier Transform Infrared Reflection−Absorption Spectroscopy: Evolution of the OH Stretch and the Dangling Bond with Film Thickness. *J. Phys. Chem. B* **2002**, *106*, 6234−6247.
(67) Dostert, K.-H.; O'Brien, C. P.; Mirabella, F.; Ivars-Barceló, F.; Schauermann, S. Adsorption of Acrolein, Propanal, and Allyl Alcohol on Pd(111): a Combined Infrared Reflection-Absorption Spectroscopy and Temperature Programmed Desorption Study. *Phys. Chem. Chem. Phys.* **2016**, *18*, 13960−13973.
(68) Browarzik, R.; Stuhl, F. Temperature Dependence of the Rate Constants for the Reactions of Oxygen Atoms with Ethene, Propene, and 1-Butene. *J. Phys. Chem.* **1984**, *88*, 6004−6009.
(69) Atkinson, R.; Pitts, J. N. Absolute Rate Constants for the Reaction of O(^{3}P) Atoms with a Series of Olefins over the Temperature Range 298−439 K. *J. Chem. Phys.* **1977**, *67*, 38−43.
(70) Ashford, R. D.; Ogryzlo, E. A. Temperature Dependence of Some Reactions of Singlet Oxygen with Olefins in the Gas Phase. *J. Am. Chem. Soc.* **1975**, *97*, 3604−3607.
(71) Cvetanovic, R. J.; Singleton, D. L. Reaction of Oxygen Atoms with Olefins. *Rev. Chem. Intermed.* **1984**, *5*, 183−226.
(72) Cvetanovic, R. J. The Biradical Intermediate in the Addition of the Ground State Oxygen Atoms, O(^{3}P), to Olefins. *J. Phys. Chem.* **1970**, *74*, 2730−2732.
(73) Leonori, F.; Occhiogrosso, A.; Balucani, N.; Bucci, A.; Petrucci, R.; Casavecchia, P. Crossed Molecular Beam Dynamics Studies of the O(^{3}P) + Allene Reaction: Primary Products, Branching Ratios, and Dominant Role of Intersystem Crossing. *J. Phys. Chem. Lett.* **2012**, *3*, 75−80.
(74) Rajak, K.; Maiti, B. Trajectory Surface Hopping Study of the O(^{3}P) + C_2H_2 Reaction Dynamics: Effect of Collision Energy on the Extent of Intersystem Crossing. *J. Chem. Phys* **2014**, *140*, 044314.
(75) Atkinson, R. Gas-Phase Tropospheric Chemistry of Volatile Organic Compounds: 1. Alkanes and Alkenes. *J. Phys. Chem. Ref. Data* **1997**, *26*, 215−290.
(76) Audouin, L.; Langlois, V.; Verdu, J.; de Bruijn, J. C. M. Role of Oxygen Diffusion in Polymer Ageing: Kinetic and Mechanical Aspects. *J. Mater. Sci.* **1994**, *29*, 569−583.
(77) Fairgrieve, S. P.; MacCallum, J. R. Diffusion-Controlled Oxidation of Polymers: A Mathematical Model. *Polym. Degrad. Stab.* **1985**, *11*, 251−265.

https://dx.doi.org/10.1021/acs.jpcc.9b11439
J. Phys. Chem. C XXXX, XXX, XXX−XXX

(78) Yousif, E. Introduction to the Photo-Oxidation Degradation Mechanisms of Polymers. In *Photostabilization of PVC: principles and applications*; Elsevier Applied Science, 2012; pp 1−41.
(79) Pawela-Crew, J.; Madix, R. J. Anomalous Effects of Weak Chemisorption on Desorption Kinetics of Alkenes: The Desorption of Propylene and Propane from Ag(110). *J. Chem. Phys.* **1996**, *104*, 1699−1708.
(80) Baker, T. A.; Xu, B.; Jensen, S. C.; Friend, C. M.; Kaxiras, E. Role of Defects in Propene Adsorption and Reaction on a Partially O-Covered Au(111) Surface. *Catal. Sci. Technol.* **2011**, *1*, 1166−1174.
(81) Nart, F. C.; Kelling, S.; Friend, C. M. Oxygen Lability on Thin Oxide Films on Mo(110)†. *J. Phys. Chem. B* **2000**, *104*, 3212−3218.
(82) Stevenson, K. P.; Kimmel, G. A.; Dohnalek, Z.; Smith, R. S.; Kay, B. D. Controlling the Morphology of Amorphous Solid Water. *Science* **1999**, *283*, 1505−1507.
(83) Gibson, K. D.; Killelea, D. R.; Becker, J. S.; Yuan, H.; Sibener, S. J. Energetic Ballistic Deposition of Volatile Gases into Ice. *Chem. Phys. Lett.* **2012**, *531*, 18−21.
(84) Kay, B. D.; Lykke, K. R.; Creighton, J. R.; Ward, S. J. The Influence of Adsorbate-Absorbate Hydrogen Bonding in Molecular Chemisorption: NH_3, HF, and H_2O on Au(111). *J. Chem. Phys.* **1989**, *91*, 5120−5121.
(85) Killelea, D. R.; Gibson, K. D.; Yuan, H.; Becker, J. S.; Sibener, S. J. Dynamics of the Sputtering of Water from Ice Films by Collisions with Energetic Xenon Atoms. *J. Chem. Phys.* **2012**, *136*, 144705.
(86) Giussani, E.; Fazzi, D.; Brambilla, L.; Caironi, M.; Castiglioni, C. Molecular Level Investigation of the Film Structure of a High Electron Mobility Copolymer via Vibrational Spectroscopy. *Macromolecules* **2013**, *46*, 2658−2670.
(87) Hayden, B. E. Reflection Absorption Infrared Spectroscopy. In *Vibrational Spectroscopy of Molecules on Surfaces*; Plenum Press, 1987; pp 267−344.
(88) Kimmel, G. A.; Stevenson, K. P.; Dohnálek, Z.; Smith, R. S.; Kay, B. D.; Smith, R. S.; Kay, B. D. Control of Amorphous Solid Water Morphology Using Molecular Beams. I. Experimental Results. *J. Chem. Phys.* **2001**, *114*, 5284−5294.
(89) Kimmel, G. A.; Dohnálek, Z.; Stevenson, K. P.; Smith, R. S.; Kay, B. D. Control of Amorphous Solid Water Morphology Using Molecular Beams. II. Ballistic Deposition Simulations. *J. Chem. Phys.* **2001**, *114*, 5295−5303.
(90) Thompson, R. S.; Brann, M. R.; Sibener, S. J. Sticking Probability of High-Energy Methane on Crystalline, Amorphous, and Porous Amorphous Ice Films. *J. Phys. Chem. C* **2019**, *123*, 17855−17863.
(91) Hudson, R. L.; Ferrante, R. F.; Moore, M. H. Infrared Spectra and Optical Constants of Astronomical Ices: I. Amorphous and Crystalline Acetylene. *Icarus* **2014**, *228*, 276−287.
(92) Manca, C.; Martin, C.; Roubin, P. Spectroscopic and Volumetric Characterization of a Non-Microporous Amorphous Ice. *Chem. Phys. Lett.* **2002**, *364*, 220−224.
(93) Cholette, F.; Zubkov, T.; Smith, R. S.; Dohnálek, Z.; Kay, B. D.; Ayotte, P. Infrared Spectroscopy and Optical Constants of Porous Amorphous Solid Water†. *J. Phys. Chem. B* **2009**, *113*, 4131−4140.
(94) Paz, Y.; Trakhtenberg, S.; Naaman, R. Reaction between $O(^3P)$ and Organized Organic Thin-Films. *J. Phys. Chem.* **1994**, *98*, 13517−13523.
(95) Paz, Y.; Trakhtenberg, S.; Naaman, R. Phase Transitions in Organized Organic Thin Films as Detected by Their Reactivity. *J. Phys. Chem.* **1993**, *97*, 9075−9077.
(96) Paz, Y.; Trakhtenberg, S.; Naaman, R. Destruction of Organized Organic Monolayers by Oxygen Atoms. *J. Phys. Chem.* **1992**, *96*, 10964−10967.
(97) Gerakines, P. A.; Hudson, R. L. Infrared Spectra and Optical Constants of Elusive Amorphous Methane. *Astrophys. J.* **2015**, *805*, L20.
(98) Alentiev, A.; Drioli, E.; Gokzhaev, M.; Golemme, G.; Ilinich, O.; Lapkin, A.; Volkov, V.; Yampolskii, Y. Gas Permeation Properties of Phenylene Oxide Polymers. *J. Memb. Sci.* **1998**, *138*, 99−107.
(99) Zhao, C.-t.; do Rosário Ribeiro, M.; De Pinho, M. N.; Subrahmanyam, V. S.; Gil, C. L.; De Lima, A. P. Structural Characteristics and Gas Permeation Properties of Polynorbornenes with Retained Bicyclic Structure. *Polymer* **2001**, *42*, 2455−2462.
(100) Kilburn, D.; Townrow, S.; Meunier, V.; Richardson, R.; Alam, A.; Ubbink, J. Organization and Mobility of Water in Amorphous and Crystalline Trehalose. *Nat. Mater.* **2006**, *5*, 632−635.
(101) Smith, R. S.; Matthiesen, J.; Knox, J.; Kay, B. D. Crystallization Kinetics and Excess Free Energy of H_2O and D_2O Nanoscale Films of Amorphous Solid Water. *J. Phys. Chem. A* **2011**, *115*, 5908−5917.
(102) Avrami, M. Kinetics of Phase Change. I General Theory. *J. Chem. Phys.* **1939**, *7*, 1103−1112.
(103) Rao, C. N. R.; Rao, K. J. *Phase Transitions in Solids: An Approach to the Study of the Chemistry and Physics of Solids*; McGraw-Hill, 1978; pp 81−95.
(104) Doremus, R. H. Difussion and Phase Change. In *Rates of Phase Transformations*; Academic Press, 1985; pp 4−31.
(105) Pradell, T.; Crespo, D.; Clavaguera, N.; Clavaguera-Mora, M. T. Diffusion Controlled Grain Growth in Primary Crystallization: Avrami Exponents Revisited. *J. Phys. Condens. Matter* **1998**, *10*, 3833−3844.
(106) Tait, S. L.; Dohnálek, Z.; Campbell, C. T.; Kay, B. D. N-Alkanes on MgO(100). II. Chain Length Dependence of Kinetic Desorption Parameters for Small n-Alkanes. *J. Chem. Phys.* **2005**, *122*, 164708.
(107) Dounce, S. M.; Mundy, J.; Dai, H.-L. Crystallization at the Glass Transition in Supercooled Thin Films of Methanol. *J. Chem. Phys.* **2007**, *126*, 191111.
(108) Gibson, K. D.; Langlois, G. G.; Li, W.; Killelea, D. R.; Sibener, S. J. Molecular Interactions with Ice: Molecular Embedding, Adsorption, Detection, and Release. *J. Chem. Phys.* **2014**, *141*, 18C514.
(109) Safarik, D. J.; Meyer, R. J.; Mullins, C. B. Thickness Dependent Crystallization Kinetics of Sub-Micron Amorphous Solid Water Films. *J. Chem. Phys.* **2003**, *118*, 4660−4671.

https://dx.doi.org/10.1021/acs.jpcc.9b11439
J. Phys. Chem. C XXXX, XXX, XXX−XXX